Proceedings of the 9ICEG
9th International Congress on Environmental Geotechnics
25-28 June, 2023 | Chania, Greece
© Authors: All rights reserved, 2023
https://doi.org/10.53243/ICEG2023-385

Centrifuge Modelling of Dynamic Compaction on Fly Ash

Vineet Gajamer[1] and B.V.S. Viswanadham[2]

[1]*Research Scholar, Department of Civil Engineering, Indian Institute of Technology Bombay, Mumbai, India, email: v.gajamer@iitb.ac.in*

[2]*Professor, Department of Civil Engineering, Indian Institute of Technology Bombay, Mumbai, India, email: viswam@civil.iitb.ac.in*

ABSTRACT

Coal is one of the major sources of energy in countries such as China, India, and the United States. The high consumption of coal with low calorific value leads to the generation of fly ash in huge quantity, which is utilized up to some extent and the rest are stored in ash ponds. Though fly ash can be used for numerous applications such as filler materials, land reclamation material, significant bearing capacity improvement is required. Also, considering the important issue of overloading and failure of ash dykes which causes significant damage to the environment, it is important to mention that the strength of deposited ash in the ponds needs to be improved before further deposition. In this study, the applicability of Dynamic Compaction (DC) on fly ash deposited in ash ponds has been investigated in a geotechnical centrifuge at 30 gravities. The model was instrumented with accelerometers which captured real-time data with a high sampling rate during the simulation. The instrumentation allowed the proper capturing of ground accelerations generated due to tamping. The test has also been further interpreted by performing Digital Image Cross-Correlation (DIC) on the images of the front elevation of the model captured during the centrifuge test. Using the DIC results, crater formations between impacts, displacement vectors and contours were plotted for qualitative assessment of the effectiveness of DC on fly ash. Through this study suitability of DC on fly ash has been investigated, and it is found that DC can effectively cause improvement in the geotechnical properties of fly ash.

Keywords: Dynamic compaction, Fly ash, Ground improvement, Centrifuge modelling

1 INTRODUCTION

Coal is one of the major sources of energy in countries such as China, India, and the United States (Bhatt et al., 2019). Industries based on coal are highly polluting and resource intensive in nature. After China, India has the second largest coal combustion rate and it contributes to 77% of the nation's total electricity generation along with lignite-based power plants (Arora, 2020). Study shows that between 2009-10 and 2018-19, approximately 64% (132 GW) growth in the power plants occurred in the country, causing more coal usage. In the last ten years, a 71% increase in the annual coal combustion rate has been recorded, resulting in a combustion rate of 629 million tonnes a year (Arora, 2020).

The increase in the consumption of coal is bound to cause an increase in the generation of fly ash and its associated problems. With such a rapid rate of urbanization, the production of coal byproducts will increase in the future and will not only occupy more area of land for storage but also lead to pollution. Most of the coal present in India is of low calorific value in the range of 3500-4000 kcal/kg, which produces less energy and high ash content (Kumar and Nandi 2021). Due to the combined effect of the high combustion rate of coal and low calorific value, the fly ash generation in India has increased from 123 million tonnes (2009-10) to 217 million tonnes (2018-19) (Arora, 2020). The byproduct of coal combustion, commonly known as fly ash, is nothing but the residue formed along with gases and is segregated either mechanically or by electrostatic precipitators. The lighter material is generally known as fly ash. The heavier unburnt residue that settles down at the base of the furnace is known as bottom ash, which constitutes about 20% of the total generated fly ash. The generated fly ash is then transported in slurry form through pipes to be stored in ash ponds.

Fly ash can be used for numerous applications such as in cement production, mine filling, brick production, land reclamation, agriculture etc. (Yousuf et al., 2020) but still, the utilization rate of fly ash in India is comparatively low (around 60%). The low rate of utilization causes piling up of unused fly ash. An estimated quantity of unused fly ash stocked in the last ten years is around 627 million tonnes (Arora., 2020). In India's context, 65,000 acres of land is estimated to be occupied by ash ponds for storage (CEA, 2022).

The high generation rate of fly ash not only causes scarcity of land for storage but also causes storage mismanagement and overloading of dykes in ash ponds causing damage to properties and inhabitants. There have been numerous cases of dyke breaches due to over dumping of ash into the ponds, such as in Nagpur (2019) and Singrauli (2020), India, causing flooding of inhabited villages, damaging agriculture, polluting major water sources and even causing casualties (Arora, 2020).

The statistics are alarming because of the land area that would be required to contain the generated fly ash in the coming future. Increasing the efficiency of storing fly ash and using them productively is crucial. Several avenues are available for improving its engineering properties to enable construction combined with other geomaterials. This will help in reducing the area needed for the storage of waste deposits and will also enhance the usability of land. Such problems highlight the need to rapidly increase the utilization rate of fly ash and also to adopt some practices to reduce the volume of stored fly ash by increasing its bearing capacity and density.

Among the various available avenues for densification, DC is one of the most economical methods, which is nonintrusive, has a large depth of improvement and is relatively less complicated in terms of equipment. The use of DC also contributes to increasing the ash pond capacity to a great extent. Very few studies on the application of DC to fly ash have been reported in the literature. Some important case studies were presented by Cui et al. (2019) and Zheng et al. (2022), where fly ash was used for the construction of road embankments by the application of DC in China.

In this study, the applicability of DC on bottom ash has been investigated in a geotechnical centrifuge at 30 gravities. The model was instrumented with accelerometers which captured real-time data with a high sampling rate during the simulation. The test has also been further interpreted by performing DIC on the images of the front elevation of the model captured during the centrifuge test. Using the DIC results, crater formations between impacts, displacement vectors and contours were plotted for qualitative assessment of the effectiveness of DC on fly ash. Through this study suitability of DC on fly ash has been investigated, and it is found that DC can effectively cause improvement in the geotechnical properties of fly ash.

2 SCALING CONSIDERATION FOR DC

In a geotechnical centrifuge, a small-scale physical model scaled down by N times is subjected to N times gravity by rotating about a vertical axis in a horizontal plane. This simulates identical stresses at homologous points in the model and the corresponding prototype. Proper scaling laws must be followed for the *N* times scaled-down model to obtain the correct values of the parameters being studied. The scaling laws for common quantities such as length, area, and volume are similar to the routine scaling laws of centrifuge modelling. Detailed derivation of parameters pertaining to DC have been shown below, where the suffix 'p' stands for prototype and 'm' stands for the model.

Mass (m)

$$m_m = \rho V_m = \rho \frac{V_p}{N^3} = \frac{m}{N^3} \quad (1)$$

V=Volume

Velocity (v)

$$v_m = \sqrt{2 g_m H_m} = \sqrt{2\, N g_p \frac{H_p}{N}} = \sqrt{2 g_p H_p} = v_p \quad (2)$$

g= acceleration due to gravity; H= Height of fall

Potential Energy (PE)

$$PE_m = m_m g_m H_m = \left(\frac{m_p}{N^3}\right)(N g_p)\left(\frac{H_p}{N}\right) = \frac{m_p g_p H_p}{N^3} = \frac{PE_p}{N^3} \quad (3)$$

Momentum

$$P_m = m_m v_m = \left(\frac{m_p}{N^3}\right)(v_p) = \frac{m_p v_p}{N^3} = \frac{P_p}{N^3} \quad (4)$$

Frequency

$$f_m = N\omega = N f_p \quad (5)$$

The scaling considerations applicable to DC have been summarized in Table 1. The time scale conflict must be addressed while modelling DC with water present in the model, as the scale factor for pore water pressure generation is *N,* and the scale factor for diffusion is N^2. This is generally adjusted by scaling the permeability by increasing the viscosity of the pore fluid by *N* times, which has been discussed and presented in detail by Kundu and Viswanadham (2021a).

Table 1*. Scaling considerations for simulating DC in a centrifuge*

Parameters	Scale factor
Time for diffusion, (s)	$1/N^2$
Mass of tamper, (t)	$1/N^3$
Radius of tamper, drop height, (m)	1/N
Time interval between drops, (s)	1/N
Frequency of drops, (s^{-1})	N
Tamper velocity, (m/s)	1
Ground acceleration, (m/s^2)	N
Ground velocity, (m/s)	1
Crater depth, (m)	1/N
Depth of improvement, (m)	1/N
Potential Energy of tamper, (t-m)	$1/N^3$
Momentum of tamper, (t-m/s)	$1/N^3$

In geotechnical centrifuge modelling, the prototype dimensions are scaled down, but the actual size of the soil particles itself are not scaled down. Similar to any modelling technique, geotechnical centrifuge modelling has some limitations as well, and the particle size effect is one of them. It is generally thought that while modelling a 40 mm-sized particle (gravel) in 100g, the model dimension of the particles should be 0.4 mm (sand). Analogously while modelling fine sand of 0.4 mm, clay of particle size of 0.004 mm should be used. However, from the basics of soil mechanics, this would adversely affect the behaviour of the material. Therefore, to model the same stress-strain behaviour, the same soil is used in the model as in the prototype (Madabhushi, 2015).

3 PROPERTIES OF MODEL MATERIAL

Bottom ash produced by M/s Dirk India, Nashik Plant situated in the Maharashtra state of India, was selected for centrifuge modelling of DC. Figure 1 shows the particle size distributions of the raw material obtained from the site and the material used for the centrifuge test.

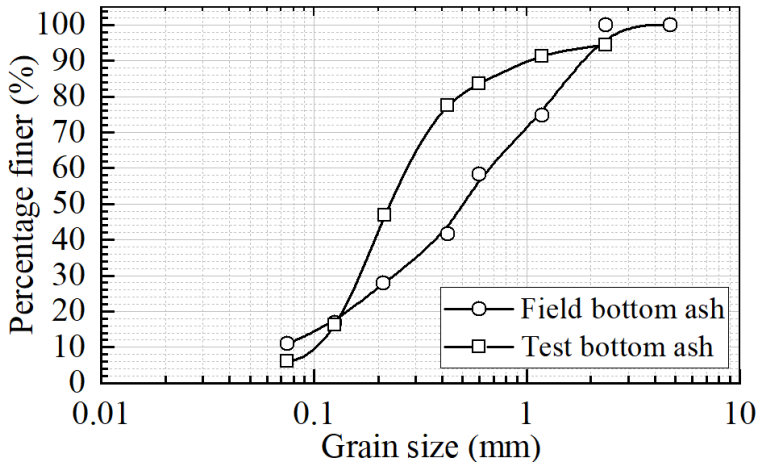


Figure 1. *Comparison of the particle size distribution of field and test bottom ash*

The raw material from the field was passed through a 2.36 mm sieve to remove the larger, coarser particles and impurities. The effective particle size *(D_{10})* of the test bottom ash, i.e., 0.075 mm, has been maintained to be close to that of the field bottom ash 0.1 mm. The test bottom ash can be classified as well-graded sand with silt (SW-SM). The details of the geotechnical properties have been summarized in Table 2.

Table 2. *Properties of the model material used in the study*

Properties	Unit	Value
Specific Gravity	--[a]	1.9
Effective particle size (D_{10})	mm	0.06
Average particle size (D_{50})	mm	0.5
Coefficient of uniformity (C_u)	--[a]	8.67
Coefficient of curvature (C_c)	--[a]	1.28
Maximum void ratio (e_{max})	--[a]	0.987
Minimum void ratio (e_{min})	--[a]	0.595
Minimum dry unit weight (γ_{min})	kN/m^3	9.38
Maximum dry unit weight (γ_{max})	kN/m^3	11.68
Hydraulic conductivity[b] (k)	m/s	7.10×10^{-4}

[a]Not relevant
[b]Constant head test on a sample placed at a relative density of 35% at normal gravity

The average particle size of the test bottom ash is 0.5 mm which is in the suitable range for the application of DC, according to Han (2015). The hydraulic conductivity can also verify the suitability of the application of DC to the bottom ash. The hydraulic conductivity was obtained as 7.10×10^{-4} m/s, experimentally through a constant head test performed on the specimen having a unit weight of 10.08 kN/m^3, corresponding to a relative density of 35%. According to Lukas (1995), the obtained hydraulic conductivity is in the acceptable range.

4 MODEL TEST PACKAGE AND TEST PROCEDURE

The study was conducted in the large beam centrifuge of 4.5 m radius and payload of 2.5 t at 100 g present at the National Geotechnical Centrifuge Facility, IIT Bombay, Mumbai, India, the details of which are presented in Chandrasekaran (2001). The test package constituted a strong box model container with an internal length of 720 mm, width of 450 mm and height of 410 mm. A Perspex sheet was used to construct the front wall of the strong box to allow viewing of the plane of symmetry of the problem (Fig. 2). On the inner side of the Perspex sheet, markers were placed to allow calibration during image analysis. A light-emitting diode frame setup arrangement was placed at the front to obtain uniform illumination, and a digital camera (Make: GoPro, USA) was used to capture images in-flight. For

measuring the induced vibration during tamping, monoaxial charge output type accelerometers (DJB Instruments, UK make) were placed at the surface, as shown in Figure 2.

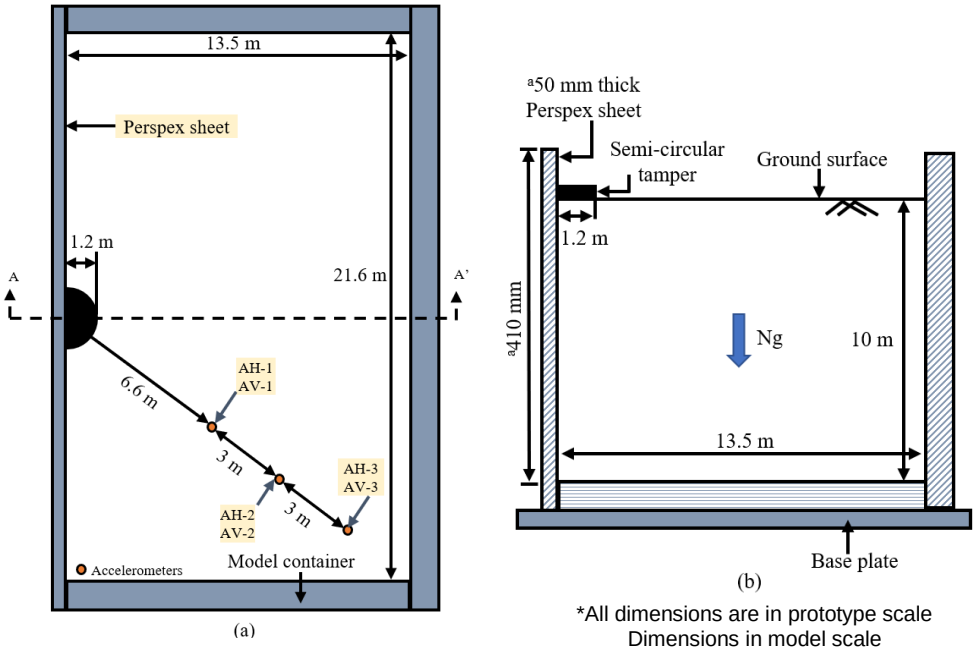


Figure 2. *Model test package and instrumentation (a) Plan view (with accelerometers at the surface of the model) (b) Cross section A-A'*

The accelerometers AH-1, AH-2 and AH-3 were placed radially to measure the horizontal/radial waves and to measure the vertical component of the waves the accelerometers AV-1, AV-2 and AV-3 were placed vertically. It was ensured that the axis of the accelerometers was oriented in the correct direction by attaching the accelerometers to a metal cube and securely placing it in the model. To impart tamping onto the model surface in-flight DC actuator developed by Kundu and Viswanadham (2021b) was used. The DC actuator is a robust one which is operated by a 24V permanent magnet direct current motor and consists of four major components, namely the impactor assembly, support system, guiding rod assembly and tamper hook arrangement. The actuator is capable of maintaining realistic time intervals between drops. The model bed was formed by air pluviation technique to achieve a dry unit weight of 10.08 kN/m^3, corresponding to 35% relative density. The height of the model was 330 mm in model dimensions, and the height of the fall was 330 mm in model dimensions as well. The tamper used was of mass 0.385 kg, which corresponds to a momentum of 10.78 kg. m/s and drop energy of 7.7 kg. m in model dimensions. The details of the test are summarised in the prototype dimension in Table 3.

Table 3. *Summary of test details in prototype dimensions*

Test ID	Model material	Dry unit weight (kN/m^3)	Mass of tamper (t)	Drop height (m)	Tamper radius (m)	Energy per blow (kg. m)	Momentum of tamper (kg. m/s)
V1	Bottom ash	10.08	20.79	10	1.2	208×10^3	291×10^3

On completion of model preparation, accelerometers were placed securely using angle arrangements at the specified locations, and the tamping assembly was mounted on the container. The container was then mounted on the swing basket, and 1 *g* readings were noted. Recording of data with a sampling rate of 20,000 samples per second was started after the completion of the equilibration time of the centrifuge was achieved.

After attaining a stable 30*g* condition, the tamping was initiated by increasing the input voltage to the motor of the DC actuator. The chosen time interval between the tamping was 3.06 s in model dimensions (1.53 min) in prototype dimensions. Sixteen impacts were allowed as there will be a marginal effect of impacts after 16 blows (Gu and Lee, 2002). After the completion of 16 blows, the motor was immediately stopped, and the initiation of stopping the centrifuge was done after 30 seconds.

5 CRATER FORMATION CAUSED BY DC

Using the high-resolution in-flight images captured after different impacts, the crater profile has been developed using ImageJ software (Ver 1.53t). The permanent markers placed at the inner side of the Perspex sheet at a horizontal distance of 160 mm and a vertical distance of 120 mm (model scale) have been used to calibrate the image space to object space. Figure 3 represents the crater depth after the 1st, 4th, 8th and 16th tamper drop along the radial distance from the centre of the tamper.

With the increase in the number of blows, it can be observed that the crater depth increases along with the radial extent of the crater. From this point onwards, the discussion has been made in terms of model dimensions followed by prototype dimensions within brackets unless specified otherwise. The maximum depth and diameter of the crater were 33.33 mm (1 m) and 160 mm (4.8 m), respectively. The crater has a flat base of radius 40 mm (1.2 m), which is equal to the radius of the tamper. From the inner centre onwards, the crater shows a symmetrical slope of around 40° until it meets the outer circle.

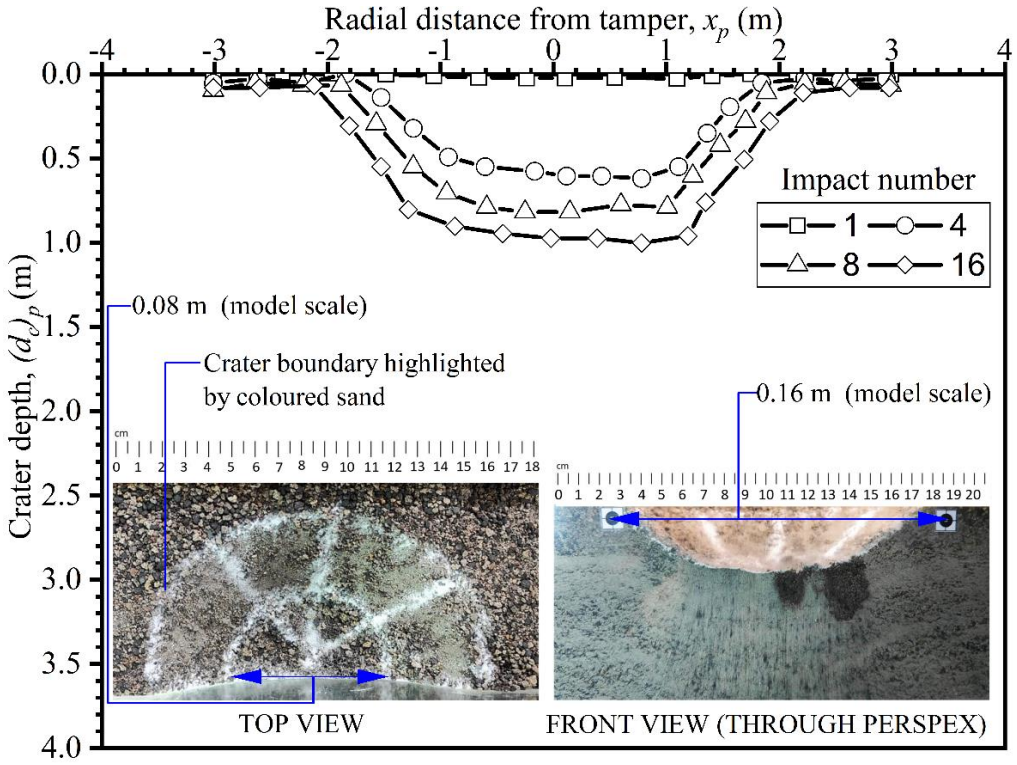


Figure 3. *Crater formed after the application of 16 blows*

6 GROUND VIBRATIONS INDUCED DUE TO DC

Due to the impact of the tamper on the ground, two types of waves, body waves and surface waves, are generated. Body waves consist of two types of waves, p-waves and *s*-waves. The *p*-waves are also known as primary, longitudinal or compressional waves due to their nature of propagation which is compression and rarefaction. The *s*-waves are also known as shear, transverse or secondary waves, and the direction of motion of the particles are perpendicular to the direction of propagation. The *s*-waves have two components, the horizontal *(SH)* and the vertical component *(SV)*. The interaction of

p-waves and *SV* waves at the surficial level creates Rayleigh waves, and the interaction of *SH* waves at the surficial layer creates love waves. The body waves are desired as they cause densification of mass, but the generated surface waves are undesirable as they can cause potential damage to the nearby structures. The surface waves attain a peak acceleration of a distance twice the thickness of the earth's crust. Considering the above discussion, it is important to monitor the ground vibrations caused due to DC to avoid any potential damage to nearby structures. Hence, the model was instrumented with accelerometers (radial and vertical) at radial distances of 220 mm (6.6 m), 320 mm (9.6 m) and 420 mm (12.6 m), as shown in Figure 4. The accelerometer data recorded were analyzed, and the absolute peak acceleration value was extracted for all the accelerometers at every tamping instance. The peak radial and vertical acceleration with radial distance from the centre of the tamper is shown in Figure 4.

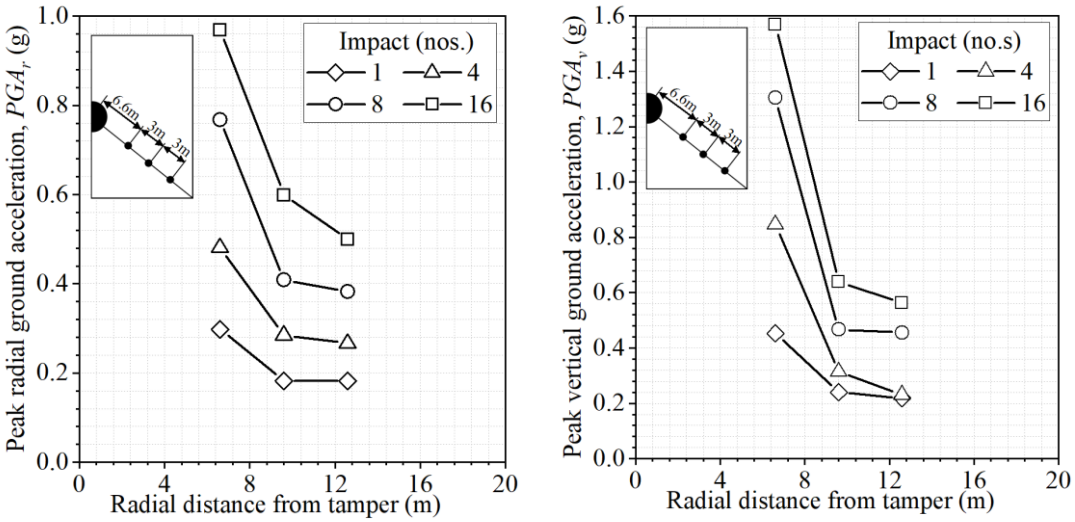


Figure 4. *Peak ground acceleration recorded by the accelerometers (a) radial (b) vertical*

The peak radial ground acceleration recorded by the closest accelerometer AH-1 at the 1st, 4th, 8th, and 16th impact is 8.94 g (0.298 g), 14.44 g (0.481 g), 23.04 g (0.768 g) and 29.1 g (0.969 g), respectively. Similarly, the peak vertical ground accelerations recorded by AV-1 at the 1st, 4th, 8th and 16th tamper drops are 13.59 g (0.453 g), 25.39 g (0.846 g), 39.13 g (1.304 g) and 47.04 g (1.568 g), respectively. The increasing trend can be observed not only for the accelerometer closest to the tamper but also by the accelerometers at a greater radial distance from the tamper (Figure 4). Further, the acceleration time histories for AH-1 and AV-1 are presented in Figure 5, which shows the ground accelerations in model and prototype dimensions at the instance of every impact.

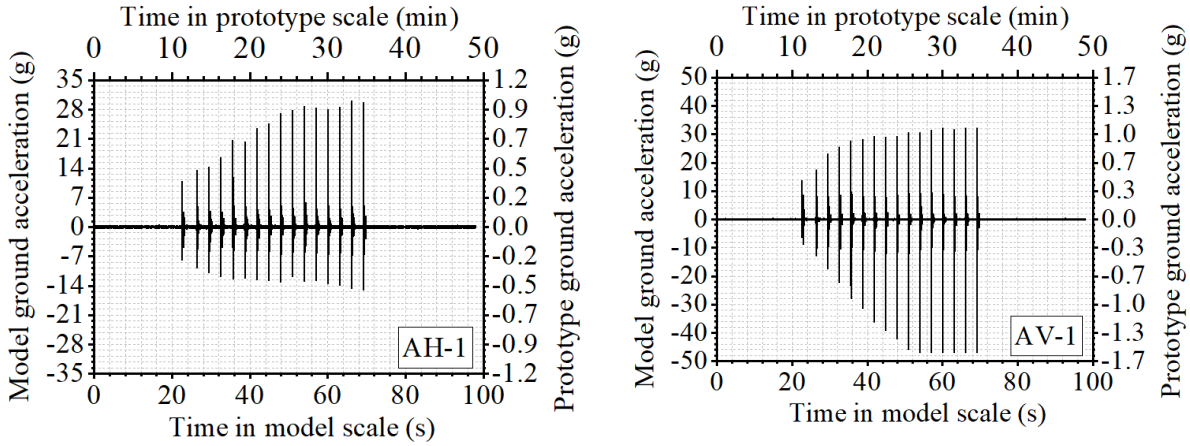


Figure 5. *Ground acceleration recorded by the accelerometers during tamping (a) radial (b) vertical*

The magnitude of accelerations progressively increases with the number of impacts signifying the gradual increase in the density of the material under compaction. This confirms the effectiveness of DC on compacting and densifying bottom ash.

7 DISPLACEMENT VECTORS AND CONTOURS FORMED DUE TO DC

GeoPIV-RG was used to obtain the vectors and displacement contours according to the procedure discussed in Stanier et al. (2015). The high-resolution images captured during the test were used as input, where a region of interest was defined, which was then discretized into a mesh of specified elemental pixel size. This was followed by estimating the movement of the mesh elements in the sequence of images, which finally gave the output as vectors corresponding to the movement of the analyzed mesh elements. The obtained vector plot is presented in Figure 6.

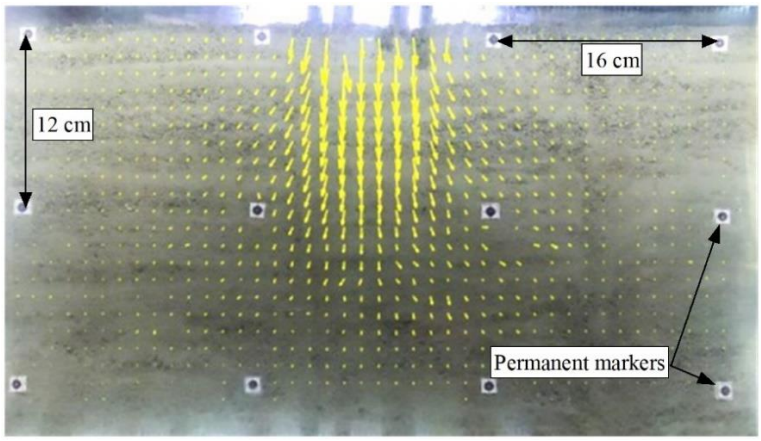


Figure 6. *Displacement vectors after completion of 16 blows*

In Figure 6, the permanent markers placed at a horizontal distance of 160 mm (4.8 m) and vertical spacing of 120 mm (4.8 m) can be seen, which are used as control points to define the region of interest and also to calibrate image space (pixels) to object space (length) for obtaining meaningful results. The obtained quiver plot was then further processed in Origin (Ver Academic 2021) to obtain the radial and vertical displacement plots, as shown in Figure 7.

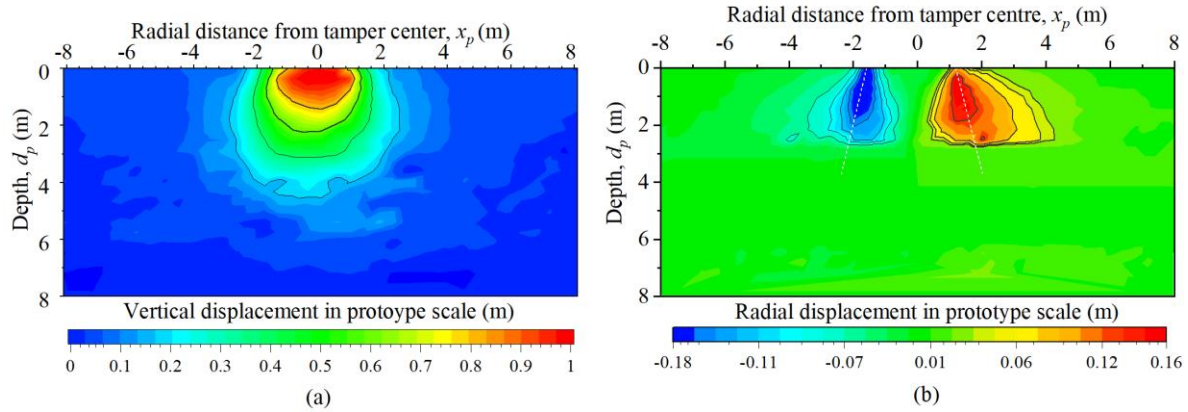


Figure 7. *Displacement contours after 16 blows (a) Vertical displacement (b) Radial displacement*

Figure 7 represents the vertical and radial displacement after the application of 16 tamper blows. It can be observed that substantial displacements have occurred in the region surrounding the tamper. The soil mass right underneath the tamper has undergone more downward vertical displacements, as can be seen from Figs. 6-7. The maximum vertical displacement plotted in Fig. 7(a) is 33.3 mm (1 m) which also matches with the results obtained by digital image analysis and the physical observations made during the post-investigation of the test. In the case of radial displacement, it can be observed that soil mass around the periphery of the tamper undergoes more radial displacement compared to vertical displacement. The progression of contour lines suggests that the radial displacement pattern almost

follows a straight line on which the displacements are maximum. On moving away from the centre line, the radial displacement reduces and is negligible at the centre and at a lateral distance of 5 m.

8 IMPROVEMENT DEPTH

Numerous researchers (Ménard and Broise, 1975; Mayne et al., 1994; Lukas, 1995) have investigated the depth of improvement in various types of soils and have estimated the value of improvement factor *'n',* which can be used to estimate the depth of improvement *(d_i)* using the following equation given by Ménard and Broise (1975):

$$d_i = n\sqrt{mH} \quad (6)$$

For the model material (SW-SM), the value of *'n'* from the literature (Mayne et al., 1984; Lukas, 1995) can be taken as 0.4 to verify the improvement depth, which calculates to be 5.76 m in the prototype scale. For verification, the test results can also be compared to the centrifuge model test (Model: TC3) carried out by Kundu and Viswanadham (2021b), which was conducted at the same DC parameters on dry sand. The maximum depth of improvement was considered till a depth where the increase in the relative density was 10%. The maximum depth of improvement was 193.3 mm (5.8 m), which corresponds to a vertical displacement of 4 mm (0.12 m). Similarly, in the present study, the vertical displacement at a depth of 192 mm (5.76 m) from Fig. 7(a) can be observed to be around 4 mm (0.12 m). Hence, it can be said that the improvement depth achieved is 192 mm (5.76 m).

9 CONCLUSIONS

The study aims to show that the material can be utilized by the application of DC for construction purposes, such as in embankments or land reclamation or for fly ash deposited in ash ponds. In the current study, centrifuge modelling of DC at 30 *g* was conducted at a tamping energy level of 208 t-m in prototype scale following proper scaling consideration. The ground accelerations at the surface of the model were recorded at different radial distances from the tamper and interpreted. It was observed that the vertical accelerations were higher compared to the induced radial acceleration. The peak ground acceleration values (radial and vertical) show a gradual increase with the progression of DC, signifying the densification of the bottom ash.

Further, the change in crater depth was estimated for 1st, 4th, 8th and 16th tamper drops using ImageJ software to understand the increment in crater depth with blow. To obtain better displacement profiles, DIC was conducted in GeoPIV-RG, using the images captured in-flight. The in-flight images were used to obtain the displacement vectors from which the radial and vertical displacements were derived. It was observed that significant vertical displacements occurred near the region underneath the centre of the tamper, whereas the maximum radial displacements occurred around the vicinity of the periphery of the tamper with negligible radial displacement under the centre of the tamper. Both radial and vertical displacements gradually decrease as the distance from the tamper increases. Using the results from the DIC and correlating the results with data from the literature, it was established that a satisfactory improvement depth of 192 mm (5.76 m) was achieved. Based on the above discussion, it can be concluded that the DC is suitable for densifying bottom ash with a satisfactory depth of improvement. Though most fly ash has trace elements comparable to that present in natural soil, attention must be paid to follow standard codes while using fly ash to ensure that the leachate concentrations are within permissible limits of drinking water quality standards (FHWA-IF-03-019). Further, studies on the effect of more fines and water table need to be carried out.

10 ACKNOWLEDGEMENTS

The authors would like to express their gratitude to the staff of the National Geotechnical Centrifuge Facility and Geotechnical Engineering Laboratory at the Indian Institute of Technology Bombay, Powai, Mumbai 400076, India, for their support in carrying out the experiment for the study.

REFERENCES

Arora, S. (2020). An Ashen Legacy: India's thermal power ash mismanagement. Centre for Science and Environment, New Delhi.

Bhatt, A., Priyadarshini, S., Mohanakrishnan A.A., Abri, A., Sattler, M., & Techapaphawit, S. (2019). Physical, chemical, and geotechnical properties of coal fly ash: A global review. Case Studies in Construction Materials, 11, e00263. https://doi.org/10.1016/J.CSCM.2019.E00263

Central Electricity Authority (CEA). (2022). Guidelines on design, construction, O&M and annual certification of coal ash ponds. (Last accessed on 15/02/2023: https://ia904708.us.archive.org/14/items/draft-guidelines-for-ash-pond/Draft_Guidelines_for_Ash_Pond.pdf)

Chandrasekaran, V. S. (2001). "Numerical and Centrifuge Modelling in Soil-Structure Interaction." Indian Geotechnical Journal, 31 (1), 1–62.

Cui, C. Y., Wang, S. J., Cui, W., & Zheng, X. (2019). Bearing Behavior of the Fly Ash Deposits on Expressway. Advances in Civil Engineering, vol: 2019 (Article ID 8450401). https://doi.org/10.1155/2019/8450401

Federal Highway Administration. 2003. Fly Ash Facts for Highway Engineers. Report no. : FHWA-IF-03-019. (https://archive.org/details/fafacts)

Gu, Q., & Lee, F. H. (2002). Ground response to dynamic compaction of dry sand. Geotechnique, 52(7), 481–493. https://doi.org/10.1680/GEOT.2002.52.7.481

Han, J. (2015). Principles and practices of ground improvement. Wiley.

Kumar, P., & Kumar Nandi, B. (2021). Combustion characteristics of high ash Indian coal, wheat straw, wheat husk and their blends. Materials Science for Energy Technologies, 4, 274–281. https://doi.org/10.1016/J.MSET.2021.08.001

Kundu, S., & Viswanadham, B. V. S. (2021a). Centrifuge Modeling and DIC of Dynamic Compaction on Sandy Soils with Shallow Water Table. Journal of Geotechnical and Geoenvironmental Engineering, 147(6): 04021037, 1-14. https://doi.org/10.1061/(asce)gt.1943-5606.0002524

Kundu, S., & Viswanadham, B. V. S. (2021b). Design and Development of an In-Flight Actuator for Modeling Dynamic Compaction in a Geotechnical Centrifuge. Geotechnical Testing Journal, 44(4), 884-911. https://doi.org/10.1520/GTJ20190169

Lukas, R. G. (1995). Dynamic Compaction, Geotechnical Engineering Circular No. 1. Federal Highway Administration, Washington D.C. https://doi.org/FHWA-SA-95-037

Madabhushi G. (2014). Centrifuge modelling for civil engineers (1st ed.). CRC Press. https://doi.org/10.1201/9781315272863

Mayne, P. W., Jones, J. S., & Dumas, J. C. (1984). Ground Response to Dynamic Compaction. Journal of Geotechnical Engineering, 110(6), 757–774. https://doi.org/10.1061/(ASCE)0733-9410(1984)110:6(757)

Ménard, L., & Broise, Y. (1975). Theoretical and Practical Aspect of Dynamic Consolidation. Geotechnique, 25(1), 3–18. https://doi.org/10.1680/geot.1975.25.1.3

Stanier, S. A., Blaber, J., Take, W. A., & White, D. J. (2016). Improved image-based deformation measurement for geotechnical applications. Canadian Geotechnical Journal, 53(5), 727–739. https://doi.org/10.1139/cgj-2015-0253

Yousuf, A., Manzoor, S. O., Youssouf, M., Malik, Z. A., & Sajjad Khawaja, K. (2020). Fly Ash: Production and Utilization in India-An Overview. Journal of Material and Environmental Science, 11(6), 911–921.

Zheng, X., Zhang, Q. Q., Wang, S. J., Wu, S. Q., & Cui, W. (2022). Performance evaluation of abandoned fly ash deposit improved by dynamic compaction for construction of highway embankment. Journal of Testing and Evaluation, 50(2). https://doi.org/10.1520/JTE20210092